A Fully Automatic Reference Deconvolution Strategy to Increase the Accuracy of In Vivo Lipid Signal Quantification

Lukas Mauch[1], Günter Steidle,[2], Jürgen Machann[2,3], Bin Yang [1], and Fritz Schick[2]

[1]Institute of Signal Processing and System Theory, Department of Electrical Engineering and Information Technology, University of Stuttgart, Stuttgart, Germany

[2]Department of Diagnostic and Interventional Radiology, Section on Experimental Radiology, University Hospital Tübingen, Tübingen, Germany

[3]Institute for Diabetes Research and Metabolic Diseases of the Helmholtz Center Munich at the University of Tübingen, German Center for Diabetes Research (DZD), Tübingen, Germany

Correspondence to:
Günter Steidle, Ph.D.
Department of Radiology
Section on Experimental Radiology
University Hospital Tübingen
Hoppe-Seyler-Straße 3
72076 Tübingen
Germany
Email: guenter.steidle@med.uni-tuebingen.de

Running title: Fully Automatic Reference Deconvolution Strategy to Improve Lipid Signal Quantification

Abstract

Purpose: Lipid signals measured by ^{1}H MR spectroscopy cannot be adequately quantified by common fitting routines like VARPRO or AMARES, if lipid spectra are distorted by irregular spatial and temporal inhomogeneities of the static magnetic field during readout. A fully automatic reference deconvolution algorithm is presented that eliminates these distortions before application of fitting routines.

Methods: The measured signal of the dominant methyl resonance is isolated with aid of a spectral estimator (ESPRIT) and used as reference signal for estimation of distortions. A Wiener filter is applied to deconvolve those distortions in the lipid spectrum. Performance of the algorithm is assessed for different bandwidths and shapes of distortions, using artificially distorted as well as measured data.

Results: Application of the fully automatic reference deconvolution algorithm on simulated spectra yields a distinct increase in quantification accuracy. Deconvolved in vivo spectra of subcutaneous fat indicate reduced spectral overlap after application of the proposed strategy.

Conclusion: The proposed method is helpful for in vivo MR spectroscopy of adipose tissue in order to correct for effects of field inhomogeneities within the voxel and for inevitable eddy current effects. Quantification accuracy is improved by eliminating distortions before application of fitting routines.

Key words: spectral overlap; reference deconvolution; Wiener filter; estimation of parameters via rotational invariance techniques algorithm

Introduction

In many clinical studies, the distribution of triglycerides, which are present in different regions of adipose tissue (e.g., layers of subcutaneous fat or visceral fat), is performed to get insight into the pathogenesis of metabolic diseases, such as type 2 diabetes (1–4). Using magnetic resonance spectroscopy (MRS) for this analysis, highly accurate quantification of the occurring signal parts is of great importance to get reliable information about the composition of body fat. Especially, precise assessment of mono- (MUFA) and polyunsaturated (PUFA) fatty acids has become an important task for metabolic studies on obesity and type 2 diabetes (3–6).

Usually, quantification of resonances in in vivo spectra is done by fitting an appropriate model of MRS signals directly to the measured data, using interactive fitting algorithms like VARPRO (7) or AMARES (8), and by extracting the estimated resonance amplitudes. A well established model for the use with VARPRO or AMARES consists of a superposition of exponentially damped complex sinusoids, which equals a superposition of Lorentzian functions in the frequency domain. However, if effects like spin-spin coupling must be taken into account, the complexity of the model increases significantly, because of the clearly increasing number of occurring complex sinusoids. In this case, the problem of signal fitting is often solved by applying LCModel (9) for quantification, which decomposes the measured data into a linear combination of model spectra from known metabolite solutions. This approach is mainly used to analyze metabolites in the brain.

However, all the mentioned methods can not fully avoid quantification errors due to spatial and temporal inhomogeneities of the static magnetic field. Spatial inhomogeneities are caused by the structural and magnetic heterogeneity of the tissue and lead to a non-exponential decay of the signal parts in time domain, which results in line broadening as well as spectral overlap in the frequency domain. Temporal inhomogeneities of the magnetic field occur due to eddy currents induced in the chassis of the MR tomograph after fast switching of field gradients necessary for volume selection. These eddy currents are known to cause a frequency modulation of the measured signal and therefore also contribute to the distortion of spectral lines. Fitting exponentially dampened sinusoids to the distorted signal, using VARPRO or AMARES, will lead to considerable errors. The usage of LCModel for spectra of adipose tissue is also limited because the measured data can not be well described by a linear combination of model spectra. Therefore, the measured data from adipose tissue is ill suited for an accurate quantification, if magnetic field inhomogeneity and eddy currents are pronounced.

More accurate quantification results are expected, if distortions caused by the static and temporal inhomogeneities were compensated in a preconditioning step. Thereafter, approved methods like VARPRO or AMARES can be used for quantification. A method to reduce the influence of eddy currents is for example the correction introduced by Klose (10), which estimates phase distortions from unsuppressed water signals. It uses the prior knowledge that the undistorted water signal

has linear phase and dominates the phase evolution of the whole signal. Major drawbacks are that this method can only be applied if water signal is dominant in the measured sample and that it can only correct distortions caused by eddy currents.

More general approaches, which do not need a water resonance and which can also counteract line broadening caused by magnetic field inhomogeneities, are spectral deconvolution algorithms like the reference deconvolution proposed in (11). Algorithms for spectral deconvolution can be used for preconditioning of the measured data prior to quantification. They can restore Lorentzian line shapes with linear phase and reduce spectral overlap in order to make the measured data better suited for the following fitting process.

In the following, a fully automatic reference deconvolution technique is presented, which is useful for preconditioning of triglyceride signals. Like described in (11), it uses the shape of an arbitrarily chosen single resonance line to estimate the actual frequency distribution produced by the spatial and temporal B_0 inhomogeneity and then deconvolves that distribution from the entire spectrum. The new approach, therefore, only needs very limited a priori information about the measured signal.

Especially if considerable spectral overlap exists, the main problem of reference deconvolution algorithms is to isolate the reference resonance from the measured data. In (11), the use of bandpass filters is proposed for this purpose. A disadvantage of this approach is that the performance of the algorithm strongly depends upon the shape of the stop- and pass-band. There is no theory how to design those filters in order to obtain the most accurate results. Furthermore, using bandpass filters, the infinitely broad Lorentzian line shape of the reference resonance will always be truncated. The newly proposed algorithm uses the Estimation of Parameters via Rotational Invariance Techniques (ESPRIT) (12) algorithm and a nearest-mean classification to isolate the reference resonance in the time domain. So choosing appropriate stop- and pass-bands can be omitted, and the reference resonance is not truncated in frequency domain.

Another difference to the algorithm proposed in (11) is that the deconvolution is performed using a Wiener filter (13) rather than simple division in time domain. Simple division leads to noise enhancement if the estimated distortion approaches zero and causes instability. The Wiener filter is a statistical approach to correct the distortion from the measured data and minimizes the mean-squared error. Therefore,

noise enhancement is kept as low as possible and stability is ensured.

Theory

Model of fat MR spectra

Because the algorithm is developed to correct the line shape of triglyceride signals, a brief overview about the known signal properties and the effects of field inhomogeneities shall be given. A triglyceride is composed of a glycerol backbone with three attached fatty acid chains. Each of those chains contains ^{1}H atoms, which can roughly be sorted in seven groups with clearly different resonance frequencies. As depicted in Fig. 1, the resulting triglyceride spectrum consists of seven dominant resonances. The chemical shifts of those resonances can be obtained from measurements and are given in Table 1 along with the nomenclature of the resonances. The sampled time signal of the methylene resonance can be well approximated by one single exponentially dampened complex sinusoid

$$s_{\mathrm{CH_2}}(n) = s_{\mathrm{CH_2}} \exp\left\{(\mathrm{j}\omega_{\mathrm{CH_2}} - \alpha_{\mathrm{CH_2}})nT_s\right\} \qquad [1]$$

with the amplitude $s_{\mathrm{CH_2}}$, dampening constant $\alpha_{\mathrm{CH_2}} = 1/T2_{\mathrm{CH_2}}$, frequency $\omega_{\mathrm{CH_2}}$ and sampling period T_s. The value of the dampening constant was chosen as $\alpha_{\mathrm{CH_2}} = 1/69\,\mathrm{ms}^{-1}$, according to in vivo measurements of T2 reported in the literature (5, 14, 15). The methylene resonance is well separated from the other resonances in the frequency domain, i.e. there are no other signal parts in the frequency range $\omega_{\mathrm{CH_2}} \pm 0.2\,\mathrm{ppm}$.

It should be mentioned that a triglyceride spectrum in general consists of more than seven resonances mentioned in Table 1 because the glycerol backbone introduces additional resonances and each signal part may exhibit multiplet characteristics due to spin-spin coupling effects. Therefore, the model for the undistorted time signal is kept as general as possible and is assumed as the superposition

$$s(n) = s_{\mathrm{CH_2}}(n) + \sum_{k=1}^{M-1} s_k \exp\left\{((\mathrm{j}\omega_k - \alpha_k)nT_s\right\} \qquad [2]$$

of the methylene resonance and $M-1$ additional dampened complex sinusoids, formed by all the remaining chemical groups. The signal order $M-1$, the amplitudes s_{CH_2} and s_k, the dampening constants α_k, as well as ω_{CH_2} and ω_k are free parameters.

Spatial inhomogeneities of the static magnetic field are considered to cause random frequency shifts $\Delta\omega$ to all M signal parts. The probability of spatial occurrence of those shifts can be described by the probability density function $p(\Delta\omega)$. The distorted signal can be derived by calculating the expected signal

$$\tilde{s}(n) = \int_{-\infty}^{\infty} \exp\left\{\mathrm{j}\Delta\omega n T_s\right\} s(n) p(\Delta\omega)\, \mathrm{d}\Delta\omega = 2\pi m(n) s(n)\ ,$$

considering all possible values of $\Delta\omega$. Because the integral has the form of an inverse Fourier Transformation, the effect of spatial inhomogeneities can be described by a multiplication of the sampled signal $s(n)$ with a non-exponentially decaying function $m(n)$, whereas $m(n) = \mathcal{F}^{-1}\left\{p(\Delta\omega)\right\}$ is the so called characteristic function of $p(\Delta\omega)$.

If eddy currents are taken into account, an additional frequency modulation is introduced (10) due to the temporal inhomogeneities of the static magnetic field. Eddy currents are in general assumed to be exponentially dampened with the relaxation time T_e. In this case, the distorted signal can be written as

$$\tilde{s}(n) = h(n) s(n) \qquad [3]$$

$$h(n) = 2\pi \exp\left\{\mathrm{j}\Phi_e(n)\right\} m(n) \qquad [4]$$

$$\Phi_e(n) = a_e \left(1 - \exp\left\{\frac{n T_s}{T_e}\right\}\right)\ , \qquad [5]$$

where a_e is an arbitrary factor depending on the strength of the eddy currents and $\Phi_e(n)$ is the time dependent phase shift caused by the eddy currents. In the frequency domain, the distorted signal can be written as the convolution $H(\omega) * S(\omega)$. So, due to the mentioned distortions, all Lorentzian signal parts are blurred likewise with an arbitrary function $H(\omega)$.

Reference Deconvolution Algorithm

Overview

The basic steps of the reference deconvolution algorithm are visualized in Fig. 2 at the example of an arbitrary MRS signal with two Lorentzian resonances. In this example the leftmost resonance is the reference resonance for which a model of the undistorted line shape exists. During measurement the signal is distorted due to the inhomogeneities of the static magnetic field (I). In a first step, the measured signal $Y(\omega)$ is decomposed into a superposition of exponentially dampened complex sinusoids. Because the example distortion $H(\omega)$ has two maximums, each resonance is split into two of such signal parts (II). Therefore, a classification and reconstruction step is needed after signal decomposition which aggregates signal parts belonging to the same resonance (III). A model of the undistorted line shape of the reference resonance is used to get an estimate $\hat{H}(\omega)$ of the distortion (IV). In a last step, the distortion is canceled by convolving the measured spectrum with an inverse of the estimated distortion (V).

Signal decomposition

Decomposition of the measured signal is performed with the ESPRIT algorithm. For reasons of simplicity, all calculations are done in time domain. Because of Eqs. 2 and 3, we know that the measured time signal $y(n)$ corresponds to a superposition of exponentially dampened complex sinusoids which is multiplied with an arbitrary non-exponentially decaying function. Therefore, it is convenient to decompose the measured signal $y(n)$ into functions of the same form. This means that $y(n)$ can be written as

$$\begin{aligned} y(n) &= \sum_{k=1}^{M} a_k \exp\{z_k n\} q_k(n) + w(n) \\ z_k &= (\mathrm{j}b_k + c_k) T_s \ , \end{aligned} \qquad [6]$$

where $q_k(n)$ represents the non-exponential decay of the k-th signal part due to inhomogeneities of the magnetic field. Because $q_k(n)$ are assumed as complex valued functions, they also cover the non-linear phase of the signal caused by eddy currents.

The signal parts which can not be decomposed remains as the rest $w(n)$.

Decomposition means to estimate the parameters a_k, z_k and $q_k(n)$. In the following, a hat ($\hat{}$) is assigned to each estimated parameter. To estimate the complex exponents z_k, the ESPRIT algorithm can be used. Therefore, N samples of the measured signal $y(0), \ldots, y(N-1)$ are arranged into the data matrix

$$\mathbf{Y} = \begin{bmatrix} y(0) & y(1) & \ldots & y(N-L) \\ y(1) & & \ldots & y(N-L+1) \\ \vdots & & & \vdots \\ y(L-1) & y(L) & \ldots & y(N-1) \end{bmatrix}$$

with column vectors of length $L > M$. Those column vectors are the measurement vectors $\mathbf{y}(l) = [y(l), y(l+1), \ldots, y(l+L-1)]^T$ at the time instants $0 \leq l \leq N-L$. If $q_k(n)$ from Eq. 6 only changes slowly in an interval of the length L it can be replaced in each measurement vector with its Taylor-series approximation. Expanding Eq. 6 around $n = l$ and just considering the constant term yields

$$y(l+n) = \sum_{k=1}^{M} a_k \exp\{z_k(l+n)\} q_k(l) + w(l+n) \; .$$

With this narrow band approximation, the data matrix $\mathbf{Y}$ can be written as

$$\mathbf{Y} \approx \mathbf{S}\mathbf{A}(\mathbf{X} \circ \mathbf{Q}) + \mathbf{W} \qquad [7]$$

with

$$
\begin{aligned}
\mathbf{A} &= \operatorname{diag}(a_1, a_2, \ldots, a_M) \\
\mathbf{S} &= \begin{bmatrix} 1 & 1 & \ldots & 1 \\ \mathrm{e}^{z_1} & \mathrm{e}^{z_2} & \ldots & \mathrm{e}^{z_M} \\ \vdots & & & \vdots \\ \mathrm{e}^{z_1(L-1)} & \mathrm{e}^{z_2(L-1)} & \ldots & \mathrm{e}^{z_M(L-1)} \end{bmatrix} \\
\mathbf{X} &= \begin{bmatrix} 1 & \mathrm{e}^{z_1} & \ldots & \mathrm{e}^{z_1(N-L)} \\ 1 & \mathrm{e}^{z_2} & \ldots & \mathrm{e}^{z_2(N-L)} \\ \vdots & \vdots & & \vdots \\ 1 & \mathrm{e}^{z_M} & \ldots & \mathrm{e}^{z_M(N-L)} \end{bmatrix} \\
\mathbf{Q} &= \begin{bmatrix} q_1(0) & q_1(1) & \ldots & q_1(N-L) \\ q_2(0) & q_2(1) & \ldots & q_2(N-L) \\ \vdots & \vdots & & \vdots \\ q_M(0) & q_M(1) & \ldots & q_M(N-L) \end{bmatrix} \\
\mathbf{W} &= \begin{bmatrix} w(0) & w(1) & \ldots & w(N-L) \\ w(1) & w(2) & \ldots & w(N-L+1) \\ \vdots & \vdots & & \vdots \\ w(L-1) & w(L) & \ldots & w(N-1) \end{bmatrix} .
\end{aligned}
$$

$\mathbf{A}$ is a diagonal matrix with the diagonal elements $a_1, \ldots, a_M$. The operator $\circ$ denotes an element-by-element matrix multiplication (Hadamard product) The product $\mathbf{A}(\mathbf{X} \circ \mathbf{Q})$ contains the M signal parts $a_k \, \mathrm{e}^{z_k n} \, q_k(n)$ in its row vectors. The matrix $\mathbf{S}$ contains the complex phase shifts between the samples of one measurement vector which are caused by time delays. In the description of the ESPRIT algorithm (12), this matrix is often referred to as steering matrix.

Applying the ESPRIT algorithm to Eq. 7 leads to the estimates $\hat{z}_k$ of the complex exponents z_k. To apply the ESPRIT algorithm, the following steps have to be performed:

- The singular value decomposition of $\mathbf{Y}$ gives the matrix $\mathbf{U}$, whose column vectors are the eigenvectors of $\mathbf{Y}\mathbf{Y}^H$, $\mathbf{Y} = \mathbf{U}\mathbf{D}\mathbf{V}$.

- The M eigenvectors $\mathbf{u_1}, \ldots, \mathbf{u_M}$ belonging to the M biggest eigenvalues are known to span the signal subspace. To calculate the parameters z_k, the signal subspace is partitioned into $\mathbf{E}_a$ and $\mathbf{E}_b$. $\mathbf{E}_a$ covers the upper $L-1$ row vectors and $\mathbf{E}_b$ is composed of the lower $L-1$ row vectors of $\mathbf{E}$.

- The estimates $\hat{z}_1, \ldots, \hat{z}_M$ are obtained by computing the logarithm of the eigenvalues of the matrix

$$\mathbf{\Psi} = -\mathbf{E}_a \mathbf{E}_b^{-1} = \mathbf{P}\mathrm{diag}\left(\mathrm{e}^{\hat{z}_1}, \ldots, \mathrm{e}^{\hat{z}_M}\right)\mathbf{P}^{-1} \ .$$

If the exponents $\hat{z}_k$ are estimated, the amplitudes a_k and the time dependent factors $q_k(n)$ can be estimated with the least squares method. Inserting the estimated $\hat{z}_k$ into $\mathbf{S}$ and $\mathbf{X}$ gives $\widehat{\mathbf{S}}$ and $\widehat{\mathbf{X}}$. The least squares estimate of the product $\mathbf{AQ}$ is given by $\widehat{\mathbf{AQ}} = (\mathbf{S}^H\mathbf{S})^{-1}\mathbf{S}^H\mathbf{Y} \circ \widehat{\mathbf{X}}^*$, where $\widehat{\mathbf{X}}^*$ is the Hadamard inverse of $\widehat{\mathbf{X}}$ or equivalently the complex conjugate of $\widehat{\mathbf{X}}$. To separate $\widehat{\mathbf{Q}}$ and the diagonal matrix $\widehat{\mathbf{A}}$, the product $\widehat{\mathbf{AQ}}$ is factorized such that the first column of $\widehat{\mathbf{Q}}$ contains only ones. This is equivalent to the assumption $q_k(0) = 1 \ \forall k$. The signal parts $\hat{s}_k(n)$ can finally be reconstructed by inserting them into $\hat{s}_k(n) = \hat{a}_k \exp\{\hat{z}_k n\}\hat{q}_k(n)$.

For the application of this decomposition, knowledge about the signal order M is necessary. It may be estimated from the measured signal using forward linear prediction or the MDL (Minimum Description Length) criterion as described in (16). Alternatively, M can be chosen experimentally by increasing the signal order until the error $w(n)$ between the measured signal $y(n)$ and its decomposition shows no further decrease.

Clustering and Reconstruction

The next step is the nearest-mean classification and the reconstruction of the reference resonance. Applying the introduced signal decomposition to a triglyceride signal leads to a result similar to case (A) of Fig. 3. As anticipated due to the distortions, each of the seven dominant resonances, including the methylene resonance, is decomposed into multiple sinusoidal signal parts. As shown in (B) of Fig. 3, the estimated signal parts can be aggregated to reconstruct the seven distorted resonances.

Therefore, each decomposed signal part $s_k(n)$ is classified, according to which of the seven resonances given in Table 1 has the closest resonance frequency. Mathematically, this means to assign class labels $\Omega_c \in \{$'methyl', 'methylene', 'β-methylene', $\ldots\}$ to all M signal parts, corresponding to the nearest-neighbor classification rule

$$\widehat{\Omega}(\hat{z}_k) \quad = \quad \arg\min_{\Omega_c} |\mathrm{Im}(\hat{z}_k) - \omega(\Omega_c)| \; \forall k \in \{1, 2, \ldots, M\} \; .$$

As class centers $\omega(\Omega_c) = \omega_c$, the center frequencies of the seven resonances in Table 1 are used. After that, the distorted methylene resonance can be reconstructed

$$\tilde{s}_{\mathrm{CH_2}}(n) = \sum_{k:\widehat{\Omega}(\hat{z}_k)=\Omega_2} \hat{s}_k(n) \; .$$

Estimate of the distortion

The estimation of the distortion is performed in the time domain by dividing the isolated reference resonance by its ideal signal model from Eq. 1:

$$\hat{h}(n) = \frac{\tilde{s}_{\mathrm{CH_2}}(n)}{s_{\mathrm{CH_2}} \exp\left\{(\mathrm{j}\omega_{\mathrm{CH_2}} - \alpha_{\mathrm{CH_2}})nT_s\right\}} \; . \qquad [8]$$

The choice of the amplitude $s_{\mathrm{CH_2}}$ only results in a scaling of $\hat{h}(n)$ and does not alter its line shape. Different values of the optimal resonance frequency $\omega_{\mathrm{CH_2}}$ have also no effect on the line shape as they only result in a phase shift of $\hat{h}(n)$. The dampening parameter $\alpha_{\mathrm{CH_2}}$ can be obtained from measurements and has influence upon the bandwidth of the estimated distortion. In this paper, $\alpha_{\mathrm{CH_2}} = 1/69\,\mathrm{ms}$ is used according to T2 values in the literature (5, 14, 15).

Wiener Filtering

The deconvolution of the measured signal is done with the Wiener filter. It is a statistical method to design an inverse to the estimated distortion which gives the best trade-off between noise suppression and signal regeneration. Under the assumptions that

- the measured signal is given by $y(n) = \hat{h}(n)s(n) + w(n)$, where $\hat{h}(n)$ is the

estimated distortion from Eq. 8

- the desired signal $s(n)$ is a non-stationary stochastic process with the power $\sigma_s^2(n)$
- the additive noise $w(n)$ is uncorrelated to $s(n)$ and has the power σ_w^2

the inverse of the signal distortion $g(n)$ is determined to minimize the mean-squared error

$$\begin{aligned} \hat{g}(n) &= \arg\min_{g(n)} \mathrm{E}\left[|s(n) - g(n)y(n)|^2\right] \\ &= \frac{\hat{h}^*(n)\sigma_s^2(n)}{|\hat{h}(n)|^2\sigma_s^2(n) + \sigma_w^2} \end{aligned} \qquad [9]$$

at each time instant n. For the special case of a noiseless measurement ($\sigma_w^2 = 0$), the inverse $g(n) = 1/\hat{h}(n)$ is simply the inverse of $\hat{h}(n)$. For noisy measurements, the signal and noise variances in the denominator of Eq. 9 ensure that the noise is enhanced as less as possible and that stability is guaranteed. Multiplying the measured signal with this inverse $s_d(n) = \hat{g}(n) \cdot y(n)$ eventually gives the deconvolved signal $s_d(n)$, where the exponential decay as well as the linear phase of each resonance are restored. This signal can be used for accurate quantification of the signal parts.

The needed noise power σ_w^2 in Eq. 9 can be estimated from the deviation between the measured data and the fitted signal model

$$\begin{aligned} w(n) &= y(n) - \sum_{\forall k} \hat{s}_k \, \mathrm{e}^{\,\hat{z}_k n} \, \hat{q}(n) \\ \hat{\sigma}_w^2 &= \frac{1}{N} \sum_{n=1}^{N} \left|w(n)\right|^2 . \end{aligned}$$

Similarly, the signal power is estimated from the fitted signal model

$$\hat{\sigma}_s^2(n) = \Big| \sum_{\forall k} \hat{s}_k \, \mathrm{e}^{\,\hat{z}_k n} \, \hat{q}(n) \Big|^2 .$$

Methods

MRS Measurements

In vitro MR spectroscopy of safflower oil

Test spectra were measured using a single-voxel stimulated echo acquisition mode (STEAM) technique on a 3 T whole body scanner (Siemens Magnetom Trio) with sequence parameters TE = 20 ms, TM = 10 ms, TR = 4 s and a voxel size of 20 × 20 × 20 mm^3. A bottle of safflower oil served as phantom. To obtain an ideal reference spectrum, the bottle was placed in the iso-center of the MRT and the position of the voxel was chosen in the center of the bottle in order to minimize the influence of spatial field inhomogeneity and eddy currents. 32 acquisitions have been acquired to obtain a good signal-to-noise ratio. This reference safflower oil spectrum is assumed as an optimal undistorted signal $s_{\mathrm{ref}}(n)$. Measurements outside the isocenter with the voxel positioned at the border of the bottle are used to test the performance of the algorithm, because field inhomogeneities and eddy currents get more pronounced. The distorted spectra have been acquired using only one acquisition in order to obtain significant noise.

In vivo MR spectroscopy of subcutaneous fat

^{1}H MR spectra were acquired from subcutaneous tissue in five male volunteers on a 3 T whole body scanner (Siemens Magnetom Trio) with a STEAM technique. Subjects were taken from a study including obese men and had a body mass index (BMI) between 27.7 and 32.2 kg/m^2. Measurement parameter were TE = 20 ms, TM = 10 ms, TR = 4 s. The size of the voxel was between 20 × 25 × 20 and 30 × 30 × 20 mm^3, dependent on the extension of subcutaneous fat and acquisition number was between 48 and 80 dependent on the voxel size.

Evaluation

Evaluation with simulated distortions

Additional to measured signals, simulated distortions are used to test the performance of the algorithm under predefined conditions. According to Eqs. 3, 4 and

5, the reference signal $s_{\mathrm{ref}}(n)$ is multiplied with an arbitrarily chosen decaying function $m(n)$ of different bandwidths to obtain an artificially distorted measurement. The signal-to-noise ratio SNR defined by $\mathrm{SNR} = 10 \cdot \log(A^2_{\mathrm{Signal}}/A^2_{\mathrm{Noise}}) = 20 \cdot \log(A_{\mathrm{Signal}}/A_{\mathrm{Noise}})$, where A_{Signal} is the signal amplitude and A_{Noise} is the amplitude of noise, is assumed to be 45 dB. The influence of the eddy currents is investigated by changing the half-life time T_e of the induced currents. The benefit of simulated distortions is, that the exact shape of the distortion is known. Therefore, it can be assessed if the distortion can be correctly estimated with the proposed algorithm.

Quadratic error as similarity measure

For performance analysis, the quadratic deviations

$$\varepsilon_y = \sum_{n=1}^{N} \left| s_{ref}(n) - y(n) \right|^2 \qquad [10]$$

$$\varepsilon_d = \sum_{n=1}^{N} \left| s_{ref}(n) - s_d(n) \right|^2 \qquad [11]$$

are calculated as similarity measures. ε_y describes the similarity between the undistorted reference signal $s_{ref}(n)$ and the measured signal $y(n)$. ε_d describes the similarity between the undistorted reference signal $s_{ref}(n)$ and the deconvolved signal $s_d(n)$. $\varepsilon_y > \varepsilon_d$ indicates that the reference deconvolution algorithm is able to approximate the original undistorted line shape.

Error of integral estimates

The performance of the blind deconvolution algorithm is assessed, using the AMARES algorithm to estimate the signal integrals from the distorted and the deconvolved signal. A number of $M = 7$ purely Lorentzian signal parts with the relative chemical shifts given in Table 1 are fitted to the signals. All estimated signal integrals $\hat{I}_1, ..., \hat{I}_7$, except $\hat{I}_3$, are normalized to the integral of the methylene resonance in order to get the integral ratios

$$v_k = \frac{\hat{I}_k}{\hat{I}_2} \,,$$

which are comparable between different measurements. As the fitting of the integral of signal s_3 was often inaccurate or incorrect due to the low amplitude and large bandwidth, the relative error for this signal was omitted in the calculations.

At first the integral ratios of the resonances in the reference signal $s_{ref}(n)$, which is the spectrum of case (C) for the simulated data and the spectrum measured in the isocenter for the in vitro data, are estimated with AMARES. Those ratios are taken as ground truth and are denoted with $v_{k,ref}$. Besides, the AMARES algorithm is used to obtain the integral ratios from the distorted and the deconvolved signal. For each of them, the error of the integral estimation

$$e_k = 100 \cdot \frac{|v_k - v_{k,\mathrm{ref}}|}{|v_{k,\mathrm{ref}}|} \,, \forall k \in [1, 7] \qquad [12]$$

can be calculated as a percentage to get a measure how accurate the integral ratio can be estimated with the AMARES algorithm.

Calculation of saturation indices (in vivo)

In in vivo MR spectra the performance of the deconvolution algorithm cannot be judged as no reference spectrum is available. Saturation indices are parameter that are generally derived from in vivo MR spectra (17). Therefore, the influence of the removal of the distortions on the accuracy of saturation (SI) and polyunsaturation indices (PUI) was examined. SI and PUI were calculated as described in (17) for both the original and the deconvolved MR spectra of the five subjects.

Results

Evaluation with simulated distortions

Evaluation of spectra with three different simulated distortions are shown in Fig. 4. From left to right, the assumed arbitrary distortion $H(\omega)$, the reference spectrum $S_{ref}(\omega)$ and the distorted spectrum $Y(\omega)$ as well as the result of deconvolution $S_d(\omega)$ are shown in the frequency domain. From top to bottom, three different cases (A) to (C) are presented. In case (A), the distortion $H(\omega)$ is assumed as a smooth function with a bandwidth of approximately 0.3 ppm. Eddy currents are assumed to decay

fast with $T_e = 50\,\text{ms}$. In case (B), a distortion with a more narrow bandwidth of approximately 0.05 ppm is assumed in combination with the same half-life T_e of the eddy currents. Case (C) shows the results if no eddy currents are present, while the distortion caused by magnetic field inhomogeneities remains the same as in case (B).

Evaluation with measured distortions (in vitro)

Similar investigations were performed by using measured distortions from voxels at the border of the safflower oil bottle. The result of those experiments are shown in Fig. 5. Because the exact distortion is not known for measured data, the estimated distortions are shown in the leftmost plots. Case (D) shows the result when the measured distortion is broadband. It is obtained from a measurement, where the voxel is far from the isocenter of the MR tomograph and encases both oil and air. Case (E) shows the behavior of the algorithm with a measured narrow band distortion.

Comparison of performance measures

The similarity measures ε_y, ε_d and the error of integral estimation e_k were calculated for the experiments of Fig. 4 and 5 as described in the Methods part. They are given in Table 2. In the first column the indexes of the four cases (A), (B), (D) and (E) are reported. The second column provides data for distorted (dist) versus deconvolved (dec) data. Deconvolution leads to a quadratic error ε_d which is between 5.3 and 89.7 times lower than the error ε_y with the distorted signal. The relative error of integral estimation e_k is in all cases except case (D) lower or similar if the deconvolved signal was used for integral estimation. Case (D) is an extreme example with broad field inhomogeneities, where the accuracy of the deconvolution algorithm drastically decreases and the narrow-bandwidth assumption is no more fulfilled. (As the fitting of the integral of the $\beta-$methylene signal is often inaccurate or incorrect due to the low amplitude and large bandwidth, the relative error for this signal is omitted in the calculations.)

Influence of the distortions bandwidth

The influence of the bandwidth of the distortion on the the deconvolution accuracy is shown in Fig. 6a. In an interval between 0.12 ppm and 0.5 ppm the mean of the quadratic errors ε_y and ε_d is calculated for eight different bandwidths of the distortion and is given in logarithmic scale. Eddy currents are not taken into account. To calculate the mean of the quadratic errors for each bandwidth, the reference signal has been successively convolved and deconvolved, assuming 100 random smooth distortions $H(\omega)$ per bandwidth. The improvement of the quadratic error lies between 7 dB for broad bandwidths and 11 dB for narrow bandwidths of the distortion.

The influence of the half-life T_e of the eddy currents on the the deconvolution accuracy is shown in Fig. 6b. In an interval between 6 ms and 100 ms the mean of the quadratic errors ε_y and ε_d is calculated for 15 different values of T_e and is given in logarithmic scale. Again, 100 random distortions $H(\omega)$ per bandwidth have been used to calculate those mean values. The improvement of the quadratic error lies between 7 dB for short T_e and 11 dB for long T_e.

Evaluation with measured distortions (in vivo)

Fig. 7 shows spectra from subcutaneous fat of all five volunteers together with the result of the reference deconvolution. In contrast to the in vitro measurements no "gold standard" is available for the integral ratios or the shape of the undistorted signal. Therefore, only an optical inspection can be made. It is obvious that the line widths of the resonances are reduced after deconvolution. The bandwidth of the resonances is reduced if the reference deconvolution algorithm is applied. Before deconvolution the methylene resonance has a bandwidth of 0.14 ppm. Deconvolution reduces the bandwidth to 0.07 ppm, what is a reduction of 50%. In the deconvolved spectrum even small side lobes caused by spin-spin coupling affects are visible because there is little spectral overlap. This can be seen in case of the methyl and the α-methylene resonance which both are examples of triplets. Elimination of eddy current distortions in the range of the methylene peak is also demonstrated in three MR spectra.

Calculation of saturation indices (in vivo)

In Table 3 the SI and the PUI for both the original and the deconvolved MR spectra (Fig. 7) together with their mean values and standard deviations are shown.

In (17) SI and PUI were calculated for a group of obese men with a BMI of 30.1 ± 1.3 kg/m^2. Mean values were SI $= 0.944 \pm 0.008$ and PUI $= 0.003 \pm 0.001$. The mean values of the SI and PUI of the deconvolved MR spectra in Table 3 are rather in the range of the values in (17) as the values of the distorted MR spectra. Furthermore the standard deviation is distinctly higher for the distorted MR spectra.

Discussion and Conclusions

The results show that the ESPRIT algorithm can be used in combination with a nearest-mean classification to isolate a reference resonance from the spectra resulting from a distorted measurement. In comparison to the selection with a bandpass filter, knowledge about the bandwidth of this reference resonance is not necessary. Furthermore, the crucial problem of determining the best suited pass- and stop-band characteristic of such a filter is omitted this way. Besides, the reference resonance is not truncated in frequency domain if the proposed algorithm is used for reference resonance isolation.

For the use of reference deconvolution algorithms with triglyceride signals, the methylene resonance can be used as a reference resonance. A signal model of the undistorted methylene resonance consisting of one single exponentially dampened complex sinusoid is sufficiently precise for an accurate estimation of the distortions line shape. For this model, only the T2 relaxation time of the methylene group is used. No informations about the amplitude or the center frequency of the methylene resonance is needed. As shown in Fig. 4, tests with simulated data reveal that the amplitude and phase response of the distortion can be accurately estimated.

Another reference deconvolution algorithm applied to lipid spectra was introduced in (18) to improve the separation of intra- and extramyocellular lipid peaks in single voxel ^{1}H MR spectroscopy. In that work, a reference spectrum acquired in tibial bone marrow was used to deconvolve the effects of the magnetic field distribution on line shape and line width of lipid spectra in lower leg skeletal musculature. Fur-

ther investigations would be necessary, whether the proposed algorithm in this work can be expanded to multiple lipid compartments of different geometry experiencing different magnetic field strength as for example skeletal musculature.

Deconvolution with a Wiener filter in the time domain is a good way to reconstruct the undisturbed signal, even if the measurements are corrupted by noise. Cases (D) and (E) show, that the Lorentzian line shapes can be restored from the distorted measurements even if only one acquisition is used during measurement and therefore noise has significant influence.

Deconvolution with the proposed algorithm in general yields an increase in quantification accuracy. The results from Table 2 show quantification with the AMARES algorithm to be clearly more stable after preconditioning with the proposed deconvolution algorithm. Visual examination of deconvolved in vivo spectra of subcutaneous fat indicates significantly reduced spectral overlap after application of the proposed algorithm. Calculated SI and PUI from the deconvolved in vivo MR spectra coincided with literature values (17) and showed less variations than the values calculated from the original data.

Different bandwidths of the distortion $h(n)$ in Fig. 6a lead to a difference in deconvolution accuracy. The algorithm works best with narrow-band distortions. This is due to the narrow-band assumptions which are used for signal decomposition. Because it is assumed that the non-exponential decay $g_k(n)$ of each signal part varies slowly in a time frame of the length L, the signal decomposition will be inaccurate if the distortions are very broadband. As a result, the estimated distortion $\hat{h}(n)$ is inaccurate and the accuracy of the deconvolution algorithm decreases.

Similar behavior can be seen investigating the influence of the half-life T_e of the eddy currents in Fig. 6b. A very fast decay of the eddy currents, e.g. $T_e < 10\,\text{ms}$, means that the eddy currents decayed immediately after excitation and have very little influence on the signal. Therefore, deconvolution accuracy is high. Fast decaying eddy currents with $10\,\text{ms} < T_e < 20\,\text{ms}$ effect a larger time interval and lead to a lower deconvolution accuracy, because $g_k(n)$ again changes fast and can not be estimated accurately during the signal decomposition. For practical applications, where eddy currents typically have a half-life of $T_e > 20\,\text{ms}$, the algorithm works highly accurate.

One may ask, how variations in the assumed value for T2 to estimate the distor-

tion $\hat{h}(n)$ will influence the deconvolution algorithm. Of course, the inverse of the assumed damping parameter α_{CH_2} should be in the range of the correct T2 value of the methylene peak in the MR spectrum of the examined adipose tissue and an accurate determination of T2 before the actual MRS measurements could be done. Actually, small deviations of the real T2 value only influence the bandwidth of the estimated distortion and not the results of the algorithm itself. Therefore, an assessment of T2 by values from literature will be sufficient in case of a determination of T2 of the investigated adipose tissue is not desirable or not possible being short of time.

References

1. Machann J, Thamer C, Schnoedt B, Stefan N, Häring H-U, Claussen CD, Fritsche A, Schick F. Hepatic lipid accumulation in healthy subjects: a comparative study using spectral fat-selective MRI and volume-localized ^{1}H-MR spectroscopy. Magn Reson Med 2006;55:913–917.

2. Machann J, Thamer C, Stefan N, Schwenzer NF, Kantartzis K, Häring H-U, Claussen CD, Fritsche A, Schick F. Follow-up whole-body assessment of adipose tissue compartments during a lifestyle intervention in a large cohort at increased risk for type 2 diabetes. Radiology 2010;257:353–363.

3. Machann J, Stefan N, Schabel C, Schleicher E, Fritsche A, Würslin C, Häring H-U, Claussen CD, Schick F. Fraction of unsaturated fatty acids in visceral adipose tissue (VAT) is lower in subjects with high total VAT volume a combined ^{1}H MRS and volumetric MRI study in male subjects. NMR Biomed 2013;26(2):232–236.

4. Schrover IM, Leiner T, Klomp DW, Wijnen JP, Uiterwaal CS, Spiering W, Visseren FL. Feasibility and reproducibility of free fatty acid profiling in abdominal adipose tissue with ^{1}H-magnetic resonance spectroscopy at 3 T: Differences between lean and obese individuals. J Magn Reson Imag 2014;40(2):423–431.

5. Hamilton G, Yokoo T, Bydder M, Cruite I, Schroeder ME, Sirlin CB, Middleton

MS. In vivo characterization of the liver fat ^{1}H MR spectrum. NMR Biomed 2011;24(7):784–790.

6. Lee Y, Jee HJ, Noh H, Kang GH, Park J, Cho J, Cho JH, Ahn S, Lee C, Kim OH, Oh BC, Kim H. In vivo ^{1}H-MRS hepatic lipid profiling in nonalcoholic fatty liver disease: An animal study at 9.4 T. Magn Reson Med 2013;70:620–629.

7. van der Veen LWC, de Beer R, Luyen PR, van Ormondt D. Accurate quantification of in vivo ^{31}P NMR signals using the variable projection method and prior knowledge. Magn Reson Med 1988;6(1):92–98.

8. Vanhamme L, van den Boogaart A, Van Huffel S. Improved method for accurate and efficient quantification of MRS data with use of prior knowledge. J Magn Reson 1997;129(1):35–43.

9. Provencher SW. Estimation of metabolite concentrations from localized in vivo proton NMR spectra. Magn Reson Med 1993;30(6):672–679.

10. Klose U. In vivo proton spectroscopy in presence of eddy currents. Magn Reson Med 1990;14(1):26–30.

11. Metz KR, Lam MM, Webb AG. Reference deconvolution: A simple and effective method for resolution enhancement in nuclear magnetic resonance spectroscopy. Conc Magn Reson 2000;12(1):21–42.

12. Roy R, Kailath T. ESPRIT–estimation of signal parameters via rotational invariance techniques. IEEE Trans Acoust Speech Signal Process 1989;37(7):984–995.

13. Wiener N. Extrapolation, interpolation, and smoothing theory of stationary time Series. New York: John Wiley & Sons; 1949.

14. Schick F, Eismann B, Jung W-I, Bongers H, Bunse M, Lutz O. Comparison of localized proton NMR signals of skeletal muscle and fat tissue in vivo: Two lipid compartments in muscle tissue. Magn Reson Med 1993;29:158–167.

15. Ren J, Dimitrov I, Dean Sherry A, Malloy CR. Composition of adipose tissue and marrow fat in humans by ^{1}H nmr at 7 Tesla. J Lipid Res 2008;49:2055–2062.

16. Reddy V, Biradar LS. SVD-based information theoretic criteria for detection of the number of damped/undamped sinusoids and their performance analysis. IEEE Trans Signal Process 1993;41(9):2872–2881.

17. Johnson NA, Walton DW, Sachinwalla T, Thompson CH, Smith K, Ruell PA, Stannard SR, George J. Noninvasive assessment of hepatic lipid composition: Advancing understanding and management of fatty liver disorders. Hepatology 2008;47:1513–1523.

18. Steidle G, Machann J, Claussen CD, Schick F. Separation of intra- and extramyocellular lipid signals in proton MR-spectra by determination of their field distribution. J Magn Reson 2002;154:228–235.

Tables

Table 1: Indices, measured chemical shifts and corresponding nomenclature of the resonances in triglyceride signals.

Index	Chem. shift ω_k	Nomenclature
1	0.90 ppm	methyl
2	1.30 ppm	methylene
3	1.59 ppm	β-methylene
4	2.03 ppm	allylic
5	2.25 ppm	α-methylene
6	2.77 ppm	diallylic
7	5.31 ppm	olefinic

Table 2: Errors of the integral estimation for the simulated data ((A) and (B)), the in vitro data ((D) and (E)) and the quotient of the quadratic errors to the reference signal for deconvolved (dec) and distorted (dist) signals.

Case	Signal	e_1	e_2	e_3	e_4	e_5	e_6	e_7	$\varepsilon_y/\varepsilon_d$
(A)	dec	11.8	0	n.a.	2.3	7.1	3.4	1.3	63.1
	dist	20.9	0	n.a.	50.1	10.0	21.2	13.7	
(B)	dec	4.8	0	n.a.	3.0	2.0	1.6	0.1	89.7
	dist	36.6	0	n.a.	16.3	6.3	4.1	2.3	
(D)	dec	27.7	0	n.a.	63.5	19.2	32.3	5.5	5.3
	dist	34.3	0	n.a.	67.1	5.9	24.3	2.0	
(E)	dec	8.6	0	n.a.	3.0	2.0	0.6	2.4	61.3
	dist	7.9	0	n.a.	3.3	6.2	1.7	4.9	

Table 3: Saturation (SI) and polyunsaturation indices (PUI) of both the original and the deconvolved MR spectra (Fig. 7). In the last column the mean values and standard deviations of the SI and PUI are shown.

Index	Signal	#1	#2	#3	#4	#5	#6	Mean
SI	dec	0.963	0.928	0.974	0.952	0.958	0.963	0.956 $\pm$ 0.016
	dist	0.950	0.928	0.797	0.935	0.862	0.947	0.903 $\pm$ 0.061
PUI	dec	0.005	0.011	0.003	0.007	0.004	0.006	0.006 $\pm$ 0.002
	dist	0.006	0.011	0.017	0.011	0.080	0.009	0.022 $\pm$ 0.028

Figures

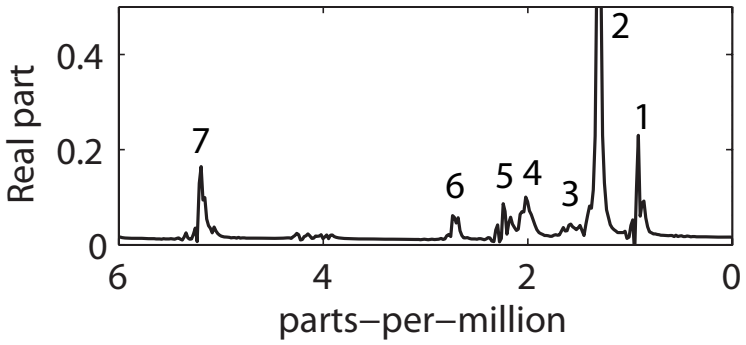

Figure 1: MR spectrum of safflower oil with labeled resonances as specified in Table 1. The spectrum was measured with a 3T whole body scanner (Siemens Magnetom Trio) using a STEAM sequence with TE = 20 ms, TM = 10 ms and TR = 1500 ms. Voxel size was $20 \times 20 \times 20$ mm^3.

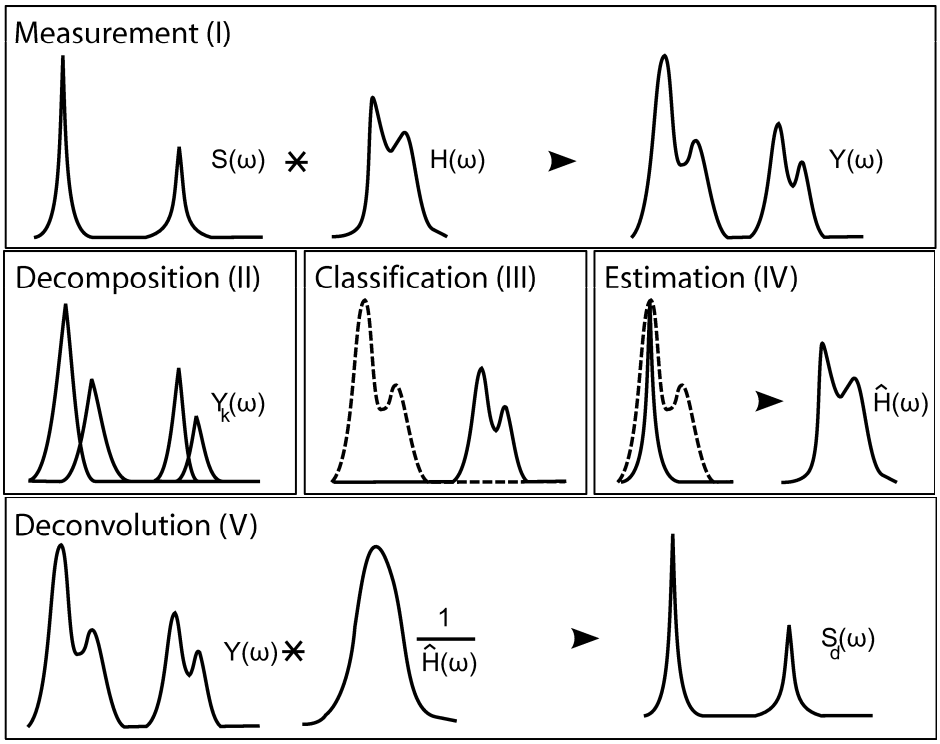

Figure 2: The reference deconvolution algorithm for a signal with two resonances: (I) The measured signal $Y(\omega)$ can be described by a convolution of the ideal signal $S(\omega)$ only determined by chemical shifts and the distortion $H(\omega)$ caused by magnetic field inhomogeneities. With aid of the ESPRIT algorithm the measured signal can be decomposed (II) in a certain number of single functions $Y_k(\omega)$, which inverse Fourier transforms are the exponentially damped complex sinusoids from Eq. 2. In a next step the nearest-mean classification (III) of the functions $Y_k(\omega)$ leads to a reconstruction of the individual distorted resonances. Now the distortion $H(\omega)$ can be estimated (IV) by dividing the extracted reference resonance by its ideal signal model from Eq. 1. Deconvolution (V) of the measured signal $Y(\omega)$ by the estimated distortion $\hat{H}(\omega)$ with aid of a Wiener filter leads to the deconvolved signal $S_d(\omega)$.

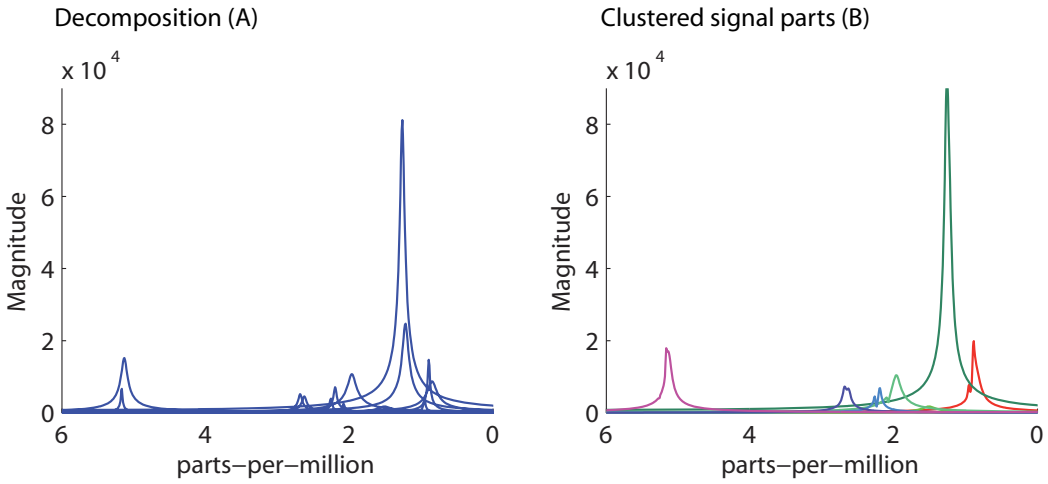

Figure 3: (A) Signal parts obtained after decomposition of the MR spectrum of safflower oil of Figure 1 with aid of the ESPRIT algorithm and (B) result of the clustering of those signal parts with aid of the nearest-mean classification to the seven dominant resonances of triglyceride signals as shown in Table 1.

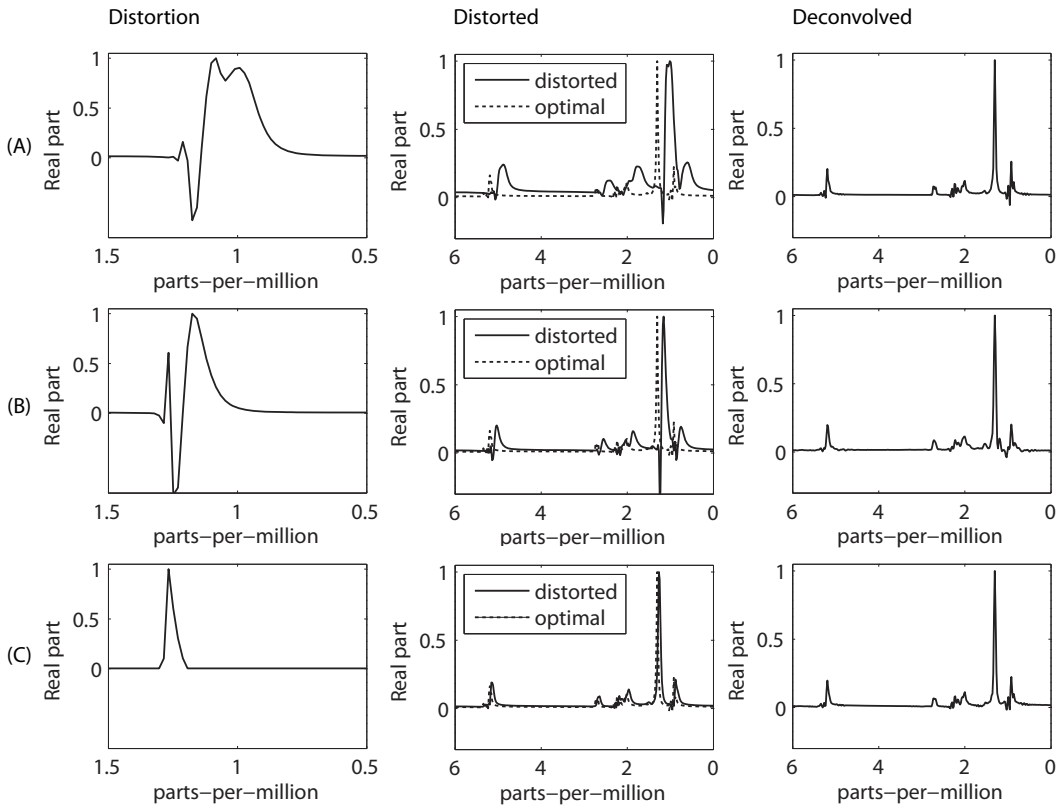

Figure 4: Three distortions (A, B and C) with different bandwidth and different influence of eddy currents shown in the left column were used to test the deconvolution algorithm for simulated data. In the middle column the original and the distorted data are depicted. The deconvolved data in the right column are practically identical with the original one.

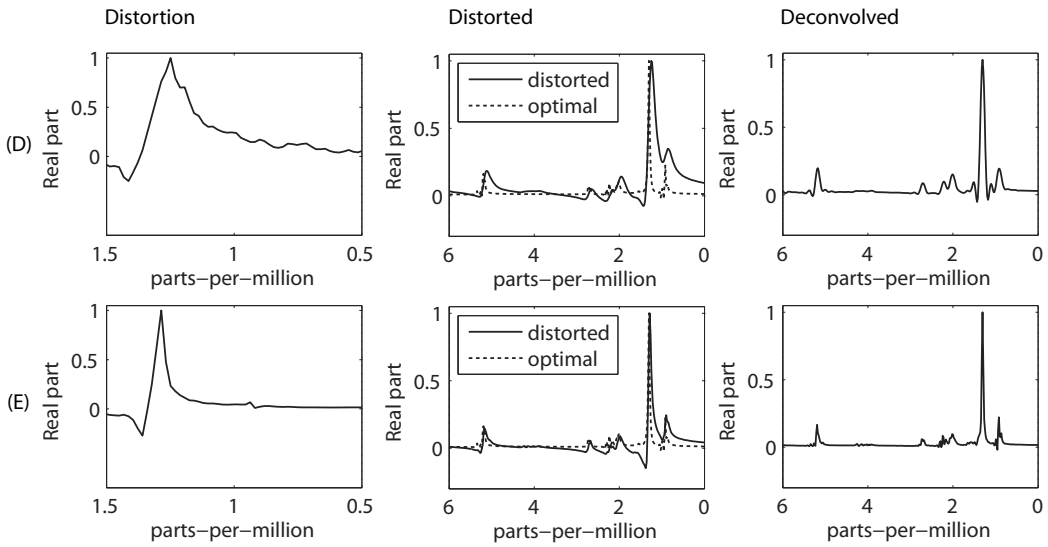

Figure 5: In the middle column two different examples (D and E) of MR spectra out of voxels positioned at the border of the bottle filled with safflower oil (solid lines) can be seen together with the optimal undistorted reference MR spectrum out of a voxel in the iso-center. The corresponding deconvolved MR spectra shown in the right column are very similar to the original reference spectrum. In the left column the corresponding estimated distortions are depicted. Effects of spatial field inhomogeneities and eddy currents are clearly visible. Especially, in case (D) the measured distortion is very broadband belonging to a voxel partially containing air from outside the bottle.

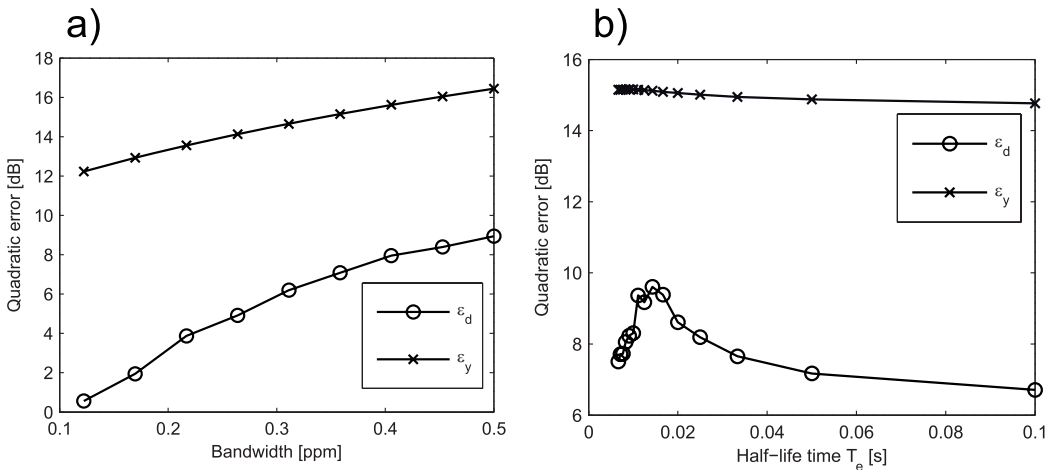

Figure 6: (a) In an interval between 0.12 ppm and 0.5 ppm the mean of the quadratic errors ε_y and ε_d was calculated for eight different bandwidths of the distortion, given in logarithmic scale. To calculate the mean of the quadratic errors for each bandwidth, the reference signal has been successively convolved and deconvolved, assuming 100 random smooth distortions $H(\omega)$ per bandwidth. The improvement of the quadratic error lies between 7 dB for broad bandwidths and 11 dB for narrow bandwidths of the distortion. (b) In an interval between 6 ms and 100 ms the mean of the quadratic errors ε_y and ε_d was calculated for 15 different values of T_e, given in logarithmic scale. To calculate the mean of the quadratic errors for each T_e, the reference signal has been successively convolved and deconvolved, assuming 100 random smooth distortions $H(\omega)$ per bandwidth. The improvement of the quadratic error lies between 7 dB for short T_e and 11 dB for long T_e.

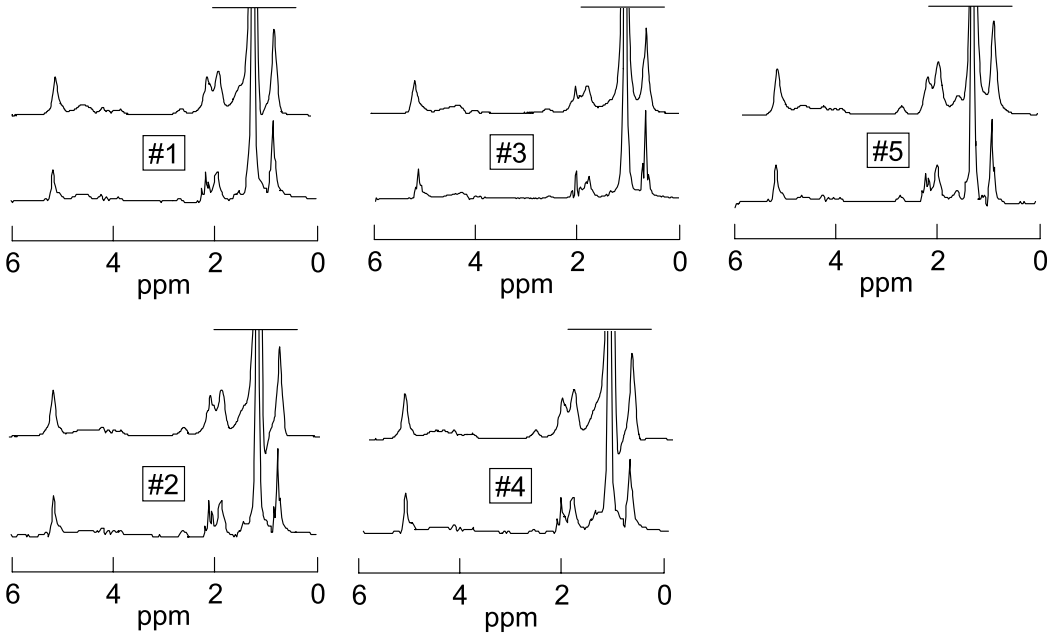

Figure 7: Examples for deconvolutions of in vivo spectra out of subcutaneous fat for all five volunteers. Above, the original, distorted spectrum is drawn and below the deconvolved one. All deconvolved spectra show distinctly smaller half widths in comparison to the original in vivo spectra. Especially elimination of eddy current distortions in the range of the methylene peak in MR spectra #2 and #4 is demonstrated. In all spectra triplet structure of the methyl and the α-methylene resonances are visualized.